IEEE Access
Multidisciplinary | Rapid Review | Open Access Journal

Received February 4, 2021, accepted February 14, 2021, date of publication February 16, 2021, date of current version March 3, 2021.

Digital Object Identifier 10.1109/ACCESS.2021.3059963

Fractional-Order Bio-Impedance Modeling for Interdisciplinary Applications: A Review

MENNA MOHSEN[1], LOBNA A. SAID[1], (Senior Member, IEEE), AHMED H. MADIAN[1,2], (Senior Member, IEEE), AHMED G. RADWAN[3,4], (Senior Member, IEEE), AND AHMED S. ELWAKIL[1,5,6], (Senior Member, IEEE)

[1]Nanoelectronics Integrated Systems Center (NISC), Nile University, Giza 12588, Egypt
[2]Radiation Engineering Department, NCRRT, Egyptian Atomic Energy Authority, Cairo 13759, Egypt
[3]Engineering Mathematics and Physics Department, Faculty of Engineering, Cairo University, Giza 12613, Egypt
[4]School of Engineering and Applied Sciences, Nile University, Giza 12588, Egypt
[5]Department of Electrical and Computer Engineering, University of Sharjah, Sharjah, United Arab Emirates
[6]Department of Electrical and Computer Engineering, University of Calgary, Calgary, AB T2N 1N4, Canada

Corresponding author: Lobna A. Said (l.a.said@ieee.org)

This work was based upon work supported by Science, Technology and Innovation Funding Authority (STIFA) under grant (#25977).

ABSTRACT Bio-impedance circuit modeling is a popular and effective non-invasive technique used in medicine and biology to fit the measured spectral impedance data of living or non-living tissues. The variations in impedance magnitude and/or phase at different frequencies reflect implicit biophysical and biochemical changes. Bio-impedance is also used for sensing environmental changes and its use in the agriculture industry is rapidly increasing. In this paper, we review and compare among the fractional-order circuit models that best fit bio-impedance data and the different methods for identifying the parameters of these circuits. Four different vegetables species (Carrot, Tomato, Zucchini, Cucumber) in three different conditions (fresh, frozen, and heated) are used to demonstrate the differences among these models.

INDEX TERMS Bio-impedance, fractional calculus, fractional-order circuits.

I. INTRODUCTION

The superiority of fractional-order modeling based on using fractional-order elements is now well-stablished across many disciplines [1]. Fractional-order models possess extra degrees of freedom that enable capturing the behavior of complex dispersive materials with fractal and fractal-like geometry (i.e. with infinitely distributed time-constants) perfectly [2]. The use of fractional calculus in the analysis of electrical circuits has also gained a lot of interest [3]–[5]. Of particular importance in this regards is the device known as the Constant Phase Element (CPE) with an impedance given by [6]:

$$Z(s) = Ks^{\alpha}, \tag{1}$$

indicating a constant voltage-current phase difference angle $\theta = \frac{\alpha\pi}{2}$. At $\alpha = (0, -1, 1)$, the CPE represents the resistor, ideal capacitor, or ideal inductor, respectively and it represents a fractional-order capacitor when $-1 < \alpha < 0$. The losses in this device are evidently frequency dependent [6] and therefore it has been used extensively in bio-impedance passive circuit models to characterize tissues and subsequently monitor their physiological changes [7].

In this review, we aim to recall the different fractional-order bio-impedance circuit models that have been presented in the literature and compare among them. Different methods for extracting the parameters of these models are also reviewed. Particular focus is given to agriculture-related applications such as freezing, heating, and thawing fruits and vegetables. A comparison between some of these models is demonstrated using four different species of vegetable (Carrot, Tomato, Zucchini, and Cucumber).

The paper is organized as follows: section II presents an overview for the bio-impedance models and their applications are discussed in Section III. Different measurement techniques are presented in Section IV. Finally, concluding remarks of this work are summarized in Section V.

II. BIO-IMPEDANCE MODELS OVERVIEW

Biological tissues have resistive, capacitive and inductive behaviors that depend on the type of tissue cellular membranes, extra-cellular resistance, intra-cellular resistance,

The associate editor coordinating the review of this manuscript and approving it for publication was Norbert Herencsar.

This work is licensed under a Creative Commons Attribution 4.0 License. For more information, see https://creativecommons.org/licenses/by/4.0/

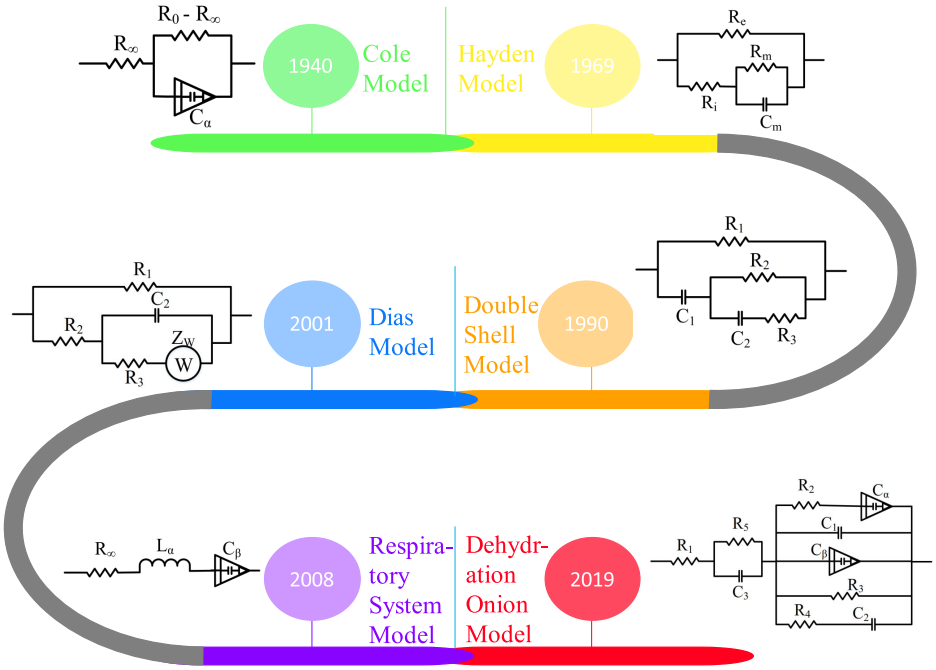

FIGURE 1. Historical overview of some of the most famous bio-impedance models.

fractal structure and morphology. Many bio-impedance models have been introduced throughout the years to accurately capture the frequency dependent impedance spectrum [8]. Figure 1 shows a brief historical overview of bio-impedance models development of the years. The Cole brothers in 1941 introduced the Cole-impedance model [9], which is similar to the model presented earlier in [10] for dielectric permittivity. The Hayden model was introduced in 1969 [11], but it showed some defects in fitting data as it neglected the vacuole representation of the tissue [12]. In 1990, the Double-Shell model was introduced in [13]–[15] to overcome the shortcomings of the Hayden model in presenting plant tissues precisely. Both the Hayden and Double-Shell models are integer-order models with respectively one and two ideal capacitors in the each of them. The Dias model was introduced in 2001 for environment modeling [16] and contains in addition to one ideal capacitor, a Warburg impedance Z_W which is a fractional-order capacitor with $\alpha = -0.5$. A mechanical representation of the human respiratory system impedance model was introduced in 2008 [17] containing for the first time a fractional-order inductor L_α in addition to the CPE C_β. In 2019, a dehydration model for onions [18] was presented. This model was more accurate compared to the Hayden and Double Shell models but also more complex since it contains three ideal capacitors and two CPEs [18]. Figure 1 clearly shows that the interest in bio-impedance modeling has been active for a long time. Many modifications have been applied to the models shown in Fig. 1 to improve their accuracy over wider frequency bands. The most important addition was to incorporate fractional-order elements which better capture the memory inherent in natural tissues which is a result of fractal geometry.

From our observations, we noticed that most bio-impedance models can be divided into two families each with three impedances. The total equivalent impedance of these two families Z_I and Z_{II} are given by

$$Z_I = Z_1 + Z_2 + Z_3, \tag{2a}$$

$$Z_{II} = \frac{Z_1(Z_2 + Z_3)}{Z_1 + (Z_2 + Z_3)}. \tag{2b}$$

Figure 2 shows some of the bio-impedance models that belong to *Family I* while Fig. 3 shows representative members of *Family II*. The symbols $C_\alpha, C_\beta, C_\gamma$ all refer to fractional-order capacitors with orders α, β, γ, respectively. A more detailed look into the two families is provided below.

A. FAMILY-I

The single dispersion Cole model shown in Fig. 2(a) is the first member of this family with an impedance given by

$$Z = R_\infty + \frac{R_0 - R_\infty}{1 + s^\alpha C_\alpha (R_0 - R_\infty)}, \tag{3}$$

where R_∞ is the resistance seen at high frequency and R_0 is the resistance seen at DC. The relaxation time constant of this model is a good measure of the heterogeneity of cell sizes and shapes [7]. A typical impedance Nyquist plot for this model is shown in Fig. 4(a) covering the frequency range 1mHz-1MHz with parameter values representing a sample apple fruit tissue.

The fractional-order Wood model shown in Fig. 2(b) has the Nyquist plot shown in Fig. 4(b) with parameters

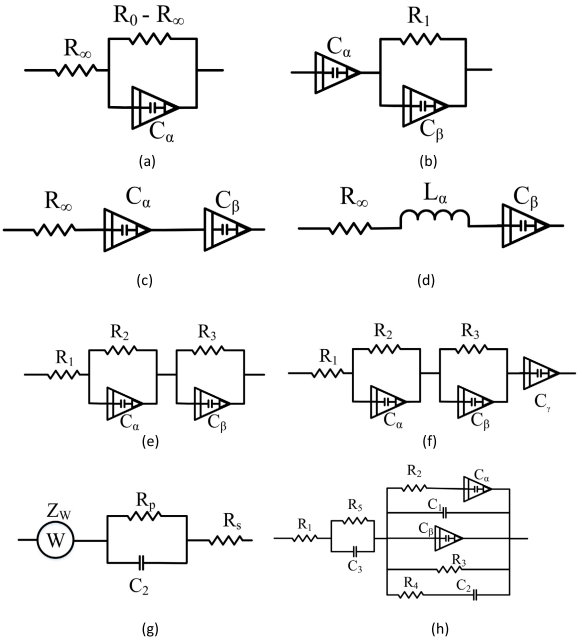

FIGURE 2. Examples of members of the *Family I* bio-impedance models: (a) single dispersion Cole model, (b) wood model, (c) electrode impedance model, (d) human respiratory model, (e) double dispersion Cole model, (f) root model, (g) fruit ripping model, and (h) onion dehydration model.

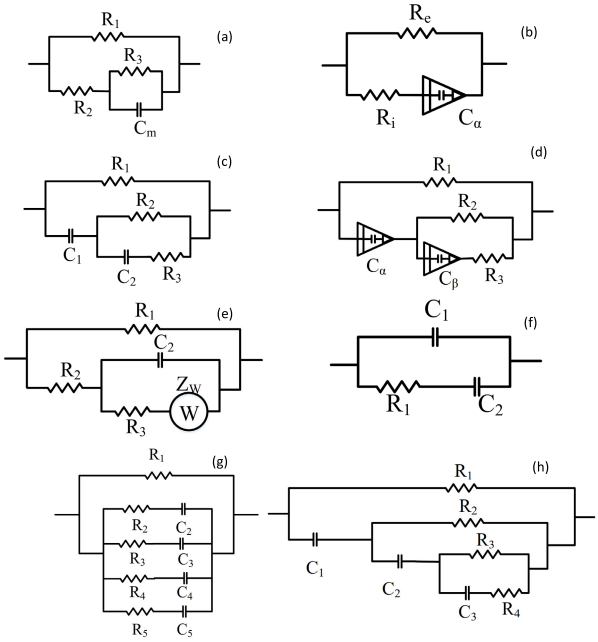

FIGURE 3. Examples of members of the *Family II* bio-impedance models: (a) Hayden model, (b) modified fractional-order Hayden model, (c) Double-Shell model, (d) fractional-order Double-Shell, (e) Dias Model, (f) Food Product Model, (g) Lumped Model, and (h) Garut Citrus Model.

representing the moisture gradients in wood tissue [19] over the frequency range 1kHz-100kHz. The electrode/tissue interface model in Fig. 2(c) has the Nyquist plots shown in Fig. 4(c) representing cardiac tissue electrode interface [20]. This model was used in [21], [22] for modeling the electrode interface in phosphate buffered saline, and implantable electrode interface in spinal cord stimulation.

The modeling of the respiratory system shown in Fig. 2(d) has the Nyquist plot shown in Fig. 4(d) with parameters reflecting human respiratory system over the frequency range 4Hz - 48Hz. Meanwhile, the double dispersion Cole-model shown in Fig. 2(e) with the performance in Fig. 4(e) corresponds to intestine tissue. The root/stem/electrode interface shown in Fig. 2(f) and its Nyquist plot in Fig. 4(f) introduced in [23] models the root fresh mass during growth. The fruit ripening model in Fig. 2(g) and its Nyquist plot in Fig. 4(g) [24] correspond to the data of the ripening of apple fruit tissue. Finally, the onion dehydration model shown in Fig. 2(h) represents the hydration of the onion tissue over the frequency range 100 Hz-200kHz [18]. The composition of each of the models in terms of the elements designated $Z_{1,2,3}$ is given on top of every Nyquist plot in Fig. 4.

B. FAMILY-II

The second family contains mainly the Hayden model shown in Fig. 3(a) with typical Nyquist plot shown in Fig. 5(a) [11] representing a banana fruit model. The modified fractional-order Hayden model is shown in Fig. 3(b) with the corresponding Nyquist plot shown in Fig. 5(b) [12] representing fresh carrot fruit tissue. The equivalent impedance of these two models is respectively

$$Z_H(s) = \frac{R_1R_2(1 + sC_1R_3 + \frac{R_3}{R_2})}{R_3 + (1 + sC_1R_3)(R_1 + R_2)}, \tag{4a}$$

$$Z_{MFOH}(s) = \frac{R_1(1 + s^{\alpha}R_2C_{\alpha})}{1 + s^{\alpha}(R_1 + R_2)C_{\alpha}}. \tag{4b}$$

Note that R_3 and C_1 are the membrane resistance and capacitance, which have been replaced by a CPE in the fractional-order version. Resistors R_2 and R_1 represent the protoplasm and apoplastic fluid resistors, respectively in the two models [11]. The integer-order Double-Shell model and its modified fractional-order version are shown in Figs. 3(c,d) with the corresponding Nyquist plots shown in Figs. 5(c,d) representing the data of banana and carrot fruits, respectively. Note that R_3 and C_2 represent the vacuole resistance and tonoplast capacitance, R_1 and R_2 represent the cell wall and cytoplasm of the tissue respectively, and C_1 is the plasma membrane capacitance.

The Dias model shown in Fig. 3(e) was used to model the measured data through electrodes spread in the bottom of the sea [16]. Figure 3(f) shows the Lumped Model, introduced in [25] for modeling the woody plant tissues. R_1 represents the extra-cellular resistance, and the parallel lumped elements represent the intra-cellular resistance. The model shown in Fig. 3(g) was used to quantify the pasteurized apple puree dilution degree [26]. The last member of this family is the Garut Citrus fruit model [27]. It represents all constituent parts of the orange fruit; R_1, R_2, R_3, and R_4 resistors represent seeds, segments, segment walls, and the outer shell,

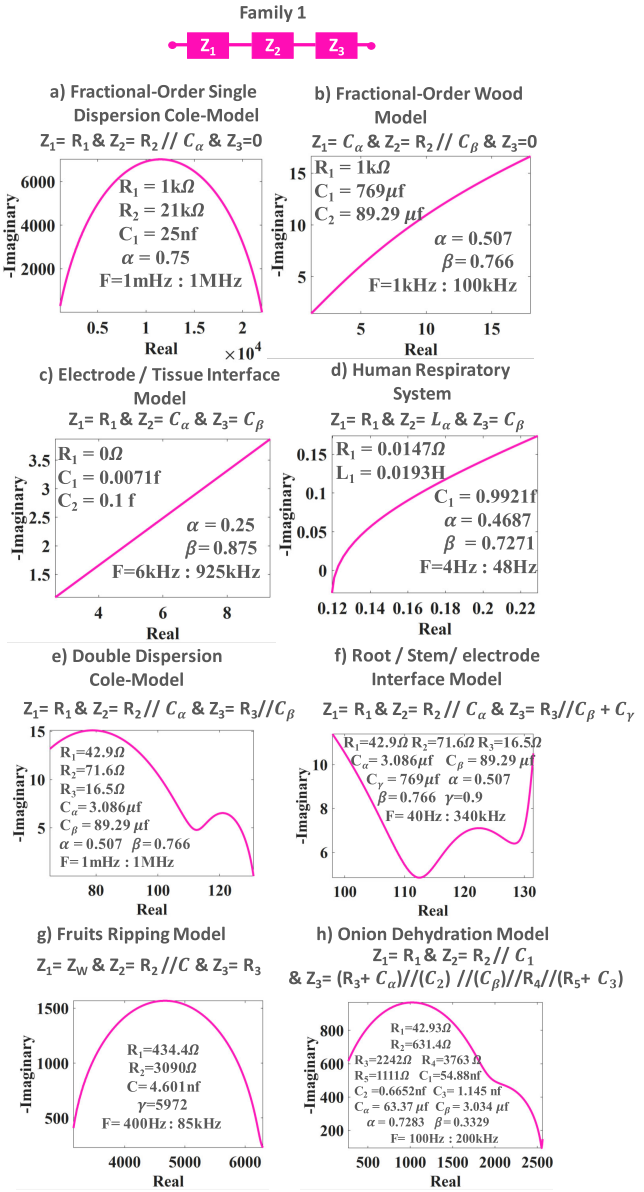

FIGURE 4. Typical Nyquist plots for the members of *Family-I*.

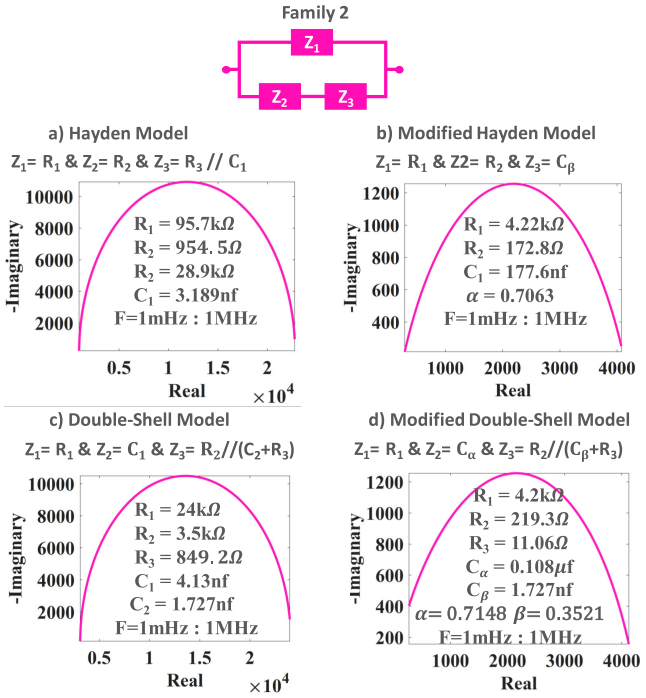

FIGURE 5. Typical Nyquist plots for some members of *Family-II* models.

respectively while C_1, C_2, and C_3 represent the segment, albedo, and flavedo, respectively.

III. APPLICATIONS OF BIO-IMPEDANCE

A. HUMAN TISSUES

Humans and animals tissues are very complex. Bio-impedance has been used on animals and humans sometimes when the organ is still alive and functioning and some other times when the organ is resected.

1) SKIN TISSUE

The human skin electrical prosperities were studied in [28]–[30] and in [31] using different electrode positions. Many circuits were tested in [30] to model the human skin, and it was found that the single dispersion Cole-model gives the best data fitting results. A new generalized element was presented in [32], [33] to better simulate the frequency dependency of the human skin by replacing the CPE in the Cole-impedance model with a GCPE (generalized CPE). The equivalent equation of the proposed generalized Cole-impedance model is

$$Z_{GCole} = R_1 + \frac{R_1 - R_2}{1 + (j\omega\tau_{\alpha^*;\beta})^{\alpha^* + \beta \log(j\omega\tau_{\alpha^*;\beta})}}, \tag{5}$$

where α^*; β are the phenomenological and physical parameters. The β parameter had a formal mathematical analogy to the γ parameter presented in [34] which describes the relaxation properties of dielectric phenomena for the medium and was derived from the general Kohlrausch-Williams-Watts relaxation law.

A diagnosis of human gender aging through skin impedance was presented in [35] using the Cole-impedance model. In [36], a study of the effect of pressure on three different skin electrodes in wearable devices was studied. The results showed that the Ag/AgCl electrodes had the lowest variations. The skin impedance model used was the Cole model and its parameter was extracted using non-linear least square fitting algorithm (NLS). Other electrodes were presented and implemented using MEMS technology in [37] and the electro-tactile of human fingers was also studied in [38] to be used in applications such as rehabilitation, telepresence and sensory substitution.

2) MUSCLE TISSUE

The single dispersion Cole-model was shown to be suitable for modeling the human bicep muscle fatigue in [39] after performing the experiment on 6 participants. The results

showed that the pre-exercise and post-exercise Cole model parameters R_1 and R_2 decreased while pseudo-capacitance increased at 72 h and 96 h post-exercise. The study concluded that the variations in the model parameters can be used to identify bicep muscle damage [39]. In [40] a study of pre- and post-execution of a fatiguing exercise protocol of biceps was conducted. The results showed an observed decrement in all Cole-impedance parameters after exercise.

Meanwhile, in [41] mice muscles were classified as healthy or not using bio-impedance. The experiments were done on thirteen different types of mice (five wild types (WT), four muscular dystrophy animals (MDX), and four amyotrophic lateral sclerosis (ALS) animals). The mice muscles' impedance were measured in a relaxed state and when they were contracted over the frequency range 1kHz-1MHz for the healthy and diseased mice. A simultaneous muscle impedance recording was done for both the force exerted by the muscle and nerve stimuli. The single dispersion Cole-model was used to identify the diseased and healthy mice through variations in its parameters. The results of [41] and [42] discussed the effects of drug therapy on healthy muscles. They used RAP-031 activin type IIB receptor at a dose of 10mg per Kg twice weekly for 16 weeks over eighteen mice (eight WT, and ten MDX). The results showed that the electrical impedance regenerated the histological and functional changes enlisted the inhibition of myostatin pathway without consideration for any differences in muscle size or volume.

3) BRAIN TISSUE

The electrical impedance effects resulting from the concentration of the electrolyte during ischemia-reperfusion injury in a rat brain was studied in [43]. Ischaemia-Reperfusion injury (IRI) is defined as the paradoxical exacerbation of cellular dysfunction and death, following the restoration of blood flow to previously ischaemic tissues. Reperfusion injury is a multi-factorial process resulting in extensive tissue destruction. The impedance was measured in the frequency range of 100Hz-35kHz using two electrodes. Four different models (Fricke-Morse, modified Fricke, Cole-impedance, and fractional Cole-model) were tested to find the best circuit parameters to reflect the IRI case. The Fricke-Morse model is a Hayden model in series with an (R//C) branch and the modified fractional-order Fricke-Morse model is a modified Hayden in series with CPE, as shown in Fig. 6. The modified Cole-impedance model gave the best representation for an IRI case, where the extracellular and intracellular ionic concentrations affect the characteristic behavior such as the conductivity, resistivity, and permeability of the brain tissue.

B. PLANT TISSUES

Bio-impedance has been used to detect and quantify ripening and aging stages, the photosynthesis process as well as thermal changes resulting from heating or freezing.

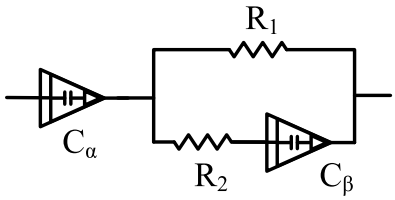

FIGURE 6. Fractional-order Fricke-Morse bio-impedance model [43].

1) PHOTOSYNTHESIS

The photosynthesis process was modeled using the Cole-impedance model in [44]. The model components represent the extra- and intra- chlorophyll space resistance and associated capacitance. The chlorophyll used extracted in a solution from Carica papaya leaves, and was tested under different lights (white, red, blue, yellow, and green). The results showed that the extra chlorophyll space resistance decreased when applying white, blue, red, and yellow lights, while it increased in the dark and under green light only.

2) RIPENING

Ripening stages and their relation to glucose concentration were investigated in [45] using a single dispersion Cole-model. The experimental materials were nine apples and nine bananas kept for thirteen days at room temperature. Bio-impedance was measured every 24 hrs along the thirteen days in the frequency range 100Hz-85kHz.

A model was introduced in [24] to capture the ripening stages of fruits and was compared with the Hyden model, Double-Shell, single and double dispersion Cole-models both integer-order and fractional-order. Figure 2(g) shows the model proposed in [24], which belongs to Family I, and has an impedance given by

$$Z = \frac{K}{\sqrt{s}} + \frac{R_p}{1 + sR_pC_2} + R_s. \tag{6}$$

The results of [24] show that the fractional-order models introduced in [12] gave the least error of fitting.

3) THERMAL AND PRESSURE EFFECTS

Physical changes in plant tissues due to heating or freezing have been studied for example in [15], [46]–[48]. In [49], a study of the freezing-thawing effect on a tube of eggplant was performed using different models and the results showed that the best model for fitting the data was the single dispersion Cole-model. In [50], the effects of heating and freezing on carrots were studied. Three samples were heated gradually to reach 90°C for an hour, and another three samples were frozen to −7°C for five hours. The bio-impedance data collected in the frequency range 0.001Hz-500kHz were fitted to a single dispersion Cole model. The study proved that the softening effect and loss of weight resulting from heating due to the reduction of the intra-cellular bonds reflected in the change in the Cole model parameter values. In particular, the decrease in the resistors' values and increase in the

CPE parameters (C_α, α) values, respectively, for all heated samples was observed. However, the frozen samples parameters showed an increase in the resistor values reflecting the hardening of the tissue [47]. As well, the CPE parameters decreased reflecting the depreciation of the air space in the cellular structure [15].

Pressure effects change not only the volume of fruits and vegetables but also their electrical and mechanical properties. In [51], high hydrostatic pressure (HHP) was applied to four different cultivate of apples for treatment. The four apples were cut into the same cube (0.0025 ± 0.0002 kg, 0.015m per side), and HHP of 100, 300, and 600 MPa was applied. The physical changes were related to bio-impedance using the fractional-order Hyden model parameters which is the best model in this type of application as concluded in many other experiments on potatoes [52], [53] and Japanese pear [54] for example. The results of applying different HHP values on the apples is to reduce the inter-cellular space which reflected directly in the decrease in the values of R_e and R_i (see Fig. 3(b)). Generally, the Hayden models have shown to be the most suitable for modeling heating, frreezing and pressure effects on tissues as can also be seen in [55] which studied the variations in moisture content of corn ear. The Double-Shell model is more suitable for modeling fruit ripening as in [56] for Kiwis.

C. COMPARISON OF MODELS

Here, we show the difference between some the surveyed models when used to fit the bio-impedance of some fruits under three conditions: fresh, heated and frozen conditions. Three models are considered for this comparison from Family I, as follows: onion dehydration model (see Fig. 2(h)), the fruit ripping model (see Fig. 2(g)), and the single dispersion Cole model (see Fig. 2(a)). Two models are considered from Family II as follows: the modified fractional-order Hayden model (see Fig. 3(b)), and the fractional-order Double-Shell (see Fig. 3(d)). Impedance was measured using an SP150 electrochemical station over the frequency range 100Hz-500kHz with 5500 points per decade in potentiostatic mode. Four fruits were selected: Carrot, Cucumber, Tomato, and Zucchini and the measured data were fitted to each of the tested models using the Randomize and Simplex optimization routine run for 5000 iterations. Two Ag/AgCl electrodes centered around the fruit sample were used in the measurements.

First, the fresh fruits were used and fitting of their measured data to the selected models done. Figures 7 and 9 show the Nyquist plots of the fitted models from Family I and Family II, respectively, compared to the actual data. Figures 8 and 10 present the extracted best fit parameter model values. From the error plots in the inset of Figs. 7 and 9, it is seen that the onion model provided the best fitting for all used fruits except for cucumber where the Cole model was better. The Ripping model is the worst for all studied fruits.

Samples of the same fruits were then frozen to $-7°$C, the impedance re-measured and the obtained Nyquist plots

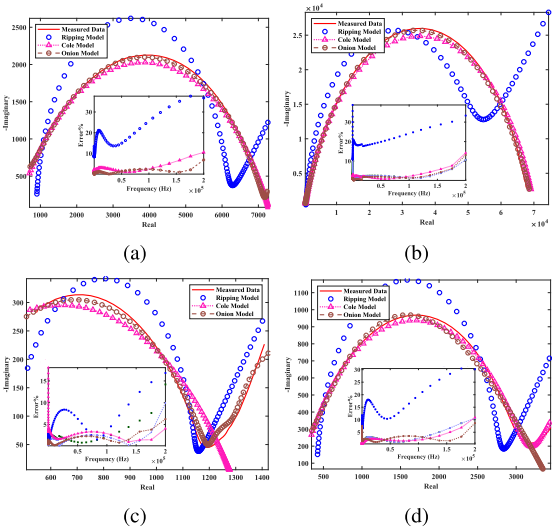

FIGURE 7. Comparison of some *Family$_I$* member models on four different *fresh* fruits (a) Carrot, (b) Tomato, (c) Zucchini, and (d) Cucumber.

Model	R_1 (Ω)	R_2 (Ω)	R_3 (Ω)	R_4 (Ω)	R_5 (Ω)	C_1 (F)	C_2 (F)	C_3 (F)	C_α (F)	C_β (F)	α	β	Z_w ($\Omega/s^{*(0.5)}$)
Ripping	434	3090	-	-	-	4.6n	-	-	-	-	-	-	5972
Cole	166	4054	-	-	-	-	-	-	0.13μ	-	0.71	-	-
Onion	43	631	2242	3763	1111	55n	0.67n	1.1n	63n	3μ	0.73	0.33	-

(a)

Model	R_1 (Ω)	R_2 (Ω)	R_3 (Ω)	R_4 (Ω)	R_5 (Ω)	C_1 (F)	C_2 (F)	C_3 (F)	C_α (F)	C_β (F)	α	β	Z_w ($\Omega/s^{*(0.5)}$)
Ripping	751	30.25k	-	-	-	1.8n	-	-	-	-	-	-	74260
Cole	299	39.20k	-	-	-	-	-	-	17.3n	-	0.79	-	-
Onion	111	10.50k	118	28.7k	666k	8.6n	2.1p	0.19n	37n	17p	0.74	0.68	-

(b)

Model	R_1 (Ω)	R_2 (Ω)	R_3 (Ω)	R_4 (Ω)	R_5 (Ω)	C_1 (F)	C_2 (F)	C_3 (F)	C_α (F)	C_β (F)	α	β	Z_w ($\Omega/s^{*(0.5)}$)
Ripping	457	211.9k	-	-	-	4n	-	-	-	-	-	-	2119
Cole	3.2p	1281	-	-	-	-	-	-	0.47μ	-	0.55	-	-
Onion	11	326	364	1388	3538	11n	0.4n	3.5μ	18.6μ	0.13μ	0.27	0.48	-

(c)

Model	R_1 (Ω)	R_2 (Ω)	R_3 (Ω)	R_4 (Ω)	R_5 (Ω)	C_1 (F)	C_2 (F)	C_3 (F)	C_α (F)	C_β (F)	α	β	Z_w ($\Omega/s^{*(0.5)}$)
Ripping	409	5658	-	-	-	5n	-	-	-	-	-	-	5658
Cole	185	3121	-	-	-	-	-	-	0.18μ	-	0.69	-	-
Onion	293	2161	48	5029	8826	78μ	2.7n	25μ	0.82μ	1.9μ	0.17	0.45	-

(d)

FIGURE 8. *Family$_I$* models parameters corresponding to Fig. 7 for four different *fresh* fruits (a) Carrot, (b) Tomato, (c) Zucchini, and (d) Cucumber. Note that $R_p = R_1, R_s = R_2$ and $R_e = R_1, R_i = R_2$.

and extracted parameters obtained, as shown in Figs. 11-14 comparing the performance of the different models. Finally, some other samples were heated and the models compared as shown in Figs. 15-18. It can be concluded from the

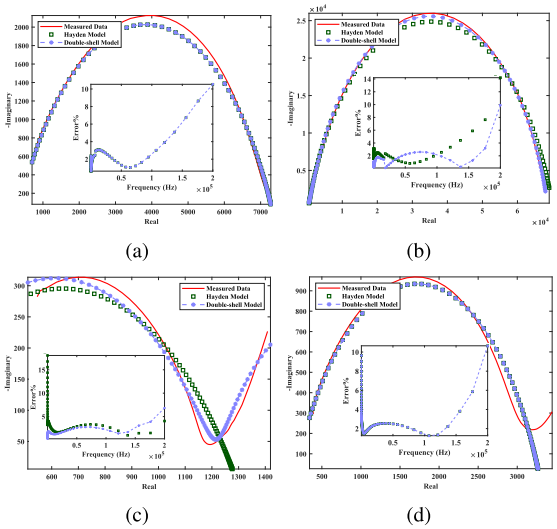

FIGURE 9. Comparison of some of *Family*$_{II}$ models for four different *fresh* fruits (a) Carrot, (b) Tomato, (c) Zucchini, and (d) Cucumber.

Model	R_1 (Ω)	R_2 (Ω)	R_3 (Ω)	C_α (F)	C_β (F)	α	β
Hayden	4220	173	-	0.18μ	-	0.71	-
Double Shell	4210	219	11	0.11μ	7.1μ	0.71	0.35

(a)

Model	R_1 (Ω)	R_2 (Ω)	R_3 (Ω)	C_α (F)	C_β (F)	α	β
Hayden	39.5k	301	-	17n	-	0.79	-
Double Shell	39.5k	301	105	17n	0.4 p	0.79	0.44

(b)

Model	R_1 (Ω)	R_2 (Ω)	R_3 (Ω)	C_α (F)	C_β (F)	α	β
Hayden	128	9p	-	0.47 μ	-	0.88	-
Double Shell	535	1527	203	0.2m	80n	0.52	0.69

(c)

Model	R_1 (Ω)	R_2 (Ω)	R_3 (Ω)	C_α (F)	C_β (F)	α	β
Hayden	3279	166.6	-	0.17 μ	-	0.69	-
Double Shell	4161	9923	147	15.3 μ	83n	0.43	0.76

(d)

FIGURE 10. *Family*$_{II}$ models parameters corresponding to Fig. 9 for four different *fresh* fruits (a) Carrot, (b) Tomato, (c) Zucchini, and (d) Cucumber. Note that $R_p = R_1$, $R_s = R_2$ and $R_e = R_1$, $R_i = R_2$.

comparison in Figs. 7, 11, and 15 that the Onion model gives the best fitting results for fresh and heated cases of the fruits from *FamilyI* while the Cole model shows better results for the frozen case. On the other hand, the Ripping model is the worst in all cases. The Hayden and Double shell models from

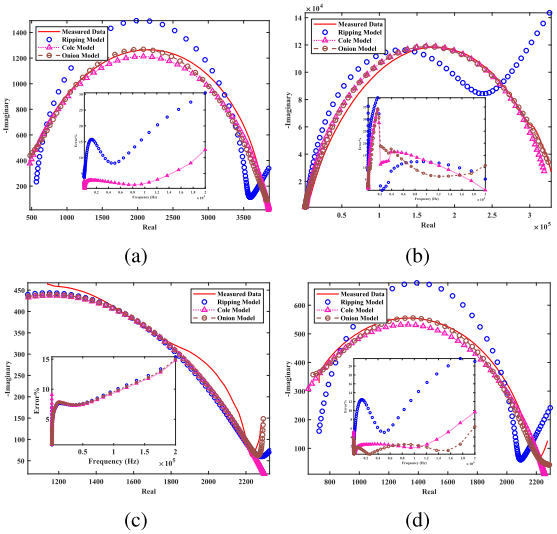

FIGURE 11. Comparison of some of *Family*$_{I}$ models for four different *frozen* fruits (a) Carrot, (b) Tomato, (c) Zucchini, and (d) Cucumber.

Model	R_1 (Ω)	R_2 (Ω)	R_3 (Ω)	R_4 (Ω)	R_5 (Ω)	C_1 (F)	C_2 (F)	C_3 (F)	C_α (F)	C_β (F)	α	β	Z_w ($\Omega s^{0.5}$)
Ripping	547	2971	-	-	-	3.4n	-	-	-	-	-	-	2670
Cole	273	3596	-	-	-	-	-	-	54n	-	0.76	-	-
Onion	51	324	4721	3748	1207	0.1μ	0.6n	1.2n	9n	16μ	0.84	0.06	-

(a)

Model	R_1 (Ω)	R_2 (Ω)	R_3 (Ω)	R_4 (Ω)	R_5 (Ω)	C_1 (F)	C_2 (F)	C_3 (F)	C_α (F)	C_β (F)	α	β	Z_w ($\Omega s^{0.5}$)
Ripping	337	187223	-	-	-	2.1n	-	-	-	-	-	-	1M
Cole	936	330171	-	-	-	-	-	-	11n	-	0.79	-	-
Onion	1421	90595	47838	248933	12G	10n	0.8n	6m	16n	18n	0.68	0.62	-

(b)

Model	R_1 (Ω)	R_2 (Ω)	R_3 (Ω)	R_4 (Ω)	R_5 (Ω)	C_1 (F)	C_2 (F)	C_3 (F)	C_α (F)	C_β (F)	α	β	Z_w ($\Omega s^{0.5}$)
Ripping	1053	1014	-	-	-	4n	-	-	-	-	-	-	1963
Cole	0.6n	2320	-	-	-	-	-	-	0.82μ	-	0.45	-	-
Onion	4	841	723	9844	1707	0.4n	0.2p	81μ	13n	1.4μ	0.8	0.48	-

(c)

Model	R_1 (Ω)	R_2 (Ω)	R_3 (Ω)	R_4 (Ω)	R_5 (Ω)	C_1 (F)	C_2 (F)	C_3 (F)	C_α (F)	C_β (F)	α	β	Z_w ($\Omega s^{0.5}$)
Ripping	708	1346	-	-	-	5n	-	-	-	-	-	-	1911
Cole	377	1886	-	-	-	-	-	-	0.2μ	-	0.65	-	-
Onion	16	689	1445	2076	6819	0.3n	4n	10μ	3μ	1.1μ	0.19	0.49	-

(d)

FIGURE 12. *Family*$_{I}$ models parameters corresponding to Fig. 11 for four different *frozen* fruits (a) Carrot, (b) Tomato, (c) Zucchini, and (d) Cucumber.

FamilyII give similar results with the Double shell slightly better in fresh fruits.

The tissue model parameters for the different circumstances change with the physiological changes in the tissues. For example in the Carrot tissue, R_1 for the Cole and Ripping models increased by a small amount from fresh to frozen phase, while R_2 decreased by a huge amount reflecting the large changes freezing has on the intra/extra- cellular resistance. The cell membrane cell capacitance decreased representing the damage that happened in the cell walls.

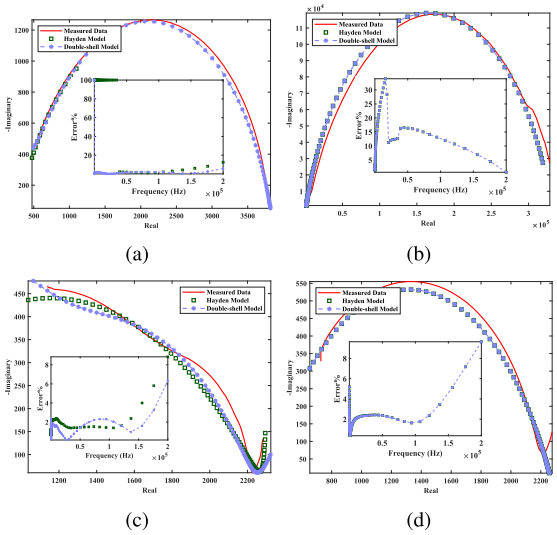

FIGURE 13. Comparison of some of $Family_{II}$ models for four different *frozen* fruits (a) Carrot, (b) Tomato, (c) Zucchini, and (d) Cucumber.

Model	R_1 (Ω)	R_2 (Ω)	R_3 (Ω)	C_α (F)	C_β (F)	α	β
Hayden	3869	293	-	47n	-	0.76	-
Double Shell	3869	1348	375	47n	1.2m	0.76	0.53

(a)

Model	R_1 (Ω)	R_2 (Ω)	R_3 (Ω)	C_α (F)	C_β (F)	α	β
Hayden	331107	938	-	10n	-	0.79	-
Double Shell	331109	9.5G	938	11n	0.7p	0.79	0.79

(b)

Model	R_1 (Ω)	R_2 (Ω)	R_3 (Ω)	C_α (F)	C_β (F)	α	β
Hayden	2320	16p	-	0.8μ	-	0.45	-
Double Shell	2289	994	0	0.3μ	0.6n	0.56	1

(c)

Model	R_1 (Ω)	R_2 (Ω)	R_3 (Ω)	C_α (F)	C_β (F)	α	β
Hayden	2263	452	-	0.15μ	-	0.65	-
Double Shell	31200	2415	478	0.4m	0.1μ	0.69	0.66

(d)

FIGURE 14. $Family_{II}$ models parameters corresponding to Fig. 13 for four different *frozen* fruits (a) Carrot, (b) Tomato, (c) Zucchini, and (d) Cucumber.

IV. BIO-IMPEDANCE MEASUREMENT TECHNIQUES

A. DIRECT METHODS

Direct methods depend on measuring bio-impedance using an impedance analyzer to obtain both the magnitude and phase of the impedance. We focus here on portable solutions like

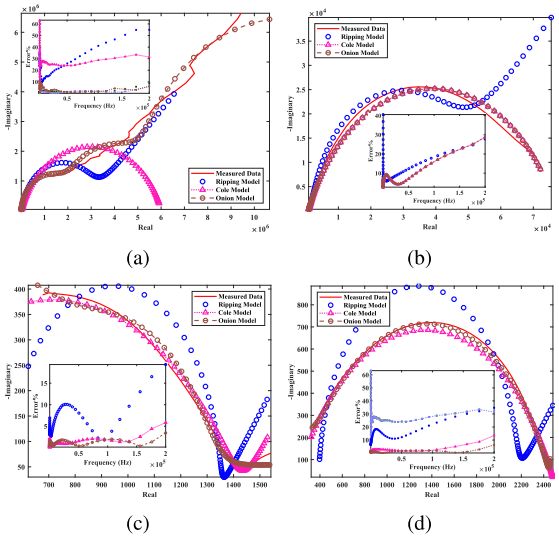

FIGURE 15. Comparison of some of $Family_I$ models for four different *heated* fruits (a) Carrot, (b) Tomato, (c) Zucchini, and (d) Cucumber.

those proposed in [37] and [57]. The AD5933 is one of the solutions used for such cheap portable devices. However, this chip has many limitations and cannot cover a bandwidth beyond 100kHz. In [58], a cheap portable device based on this chip was introduced (see Fig. 19) and used to monitor Zucchini growing stages. The measured impedance data is transmitted wirelessly to a base station. In [59], a system using this chip was also used in monitoring the strawberry aging and in [45] for banana ripening monitoring. Meanwhile, a device based on a Raspberry Pi solution was developed in [60]. Another system was presented in [61] targeting the banana fruit market through enabling remote quality monitoring using a WSN-based architecture. Artificial Neural Networks (ANNs) were used for classification and decision making.

Due to the large number of potential applications in agriculture, [62] proposed another possible system. [63], proposed a multi-frequency multi-source bio-impedance measurement technique.

B. INDIRECT METHODS

In [64]–[66] bio-impedance model parameters were extracted using the measured magnitude response only resulting from step-current excitation. By recording the step response in the time-domain of the tissue, an optimization routine can be used to fit the measured data to a readily known closed-from response obtained with an assumed a-priori circuit model. In a similar manner, the double dispersion Cole-impedance model parameters were extracted using the magnitude-only response in [67].

The magnitude-only method was also applied in [68], [69], where the parameters were extracted from a filter response with fruit tissue embedded as a component inside the filter. The effects of electrode locations on the extracted model parameters was studied in [68], [70]. Indirect impedance

Model	R_1 (Ω)	R_2 (Ω)	R_3 (Ω)	R_4 (Ω)	R_5 (Ω)	C_1 (F)	C_2 (F)	C_3 (F)	C_α (F)	C_β (F)	α	β	Z_w ($\Omega s^\alpha(\Omega.S)$)
Ripping	19p	2643k	-	-	-	33p	-	-	-	-	-	-	31010 k
Cole	0.1n	6011k	-	-	-	-	-	-	0.3n	-	0.79	-	-
Onion	1517	0.2n	7043k	33010k	5964k	0	19p	41p	2.3n	2.3n	0.78	0.38	-

(a)

Model	R_1 (Ω)	R_2 (Ω)	R_3 (Ω)	R_4 (Ω)	R_5 (Ω)	C_1 (F)	C_2 (F)	C_3 (F)	C_α (F)	C_β (F)	α	β	Z_w ($\Omega s^\alpha(\Omega.S)$)
Ripping	620	36051	-	-	-	12n	-	-	-	-	-	-	308K
Cole	727	76423	-	-	-	-	-	-	83n	-	0.74	-	-
Onion	154	30613	642	55752	8831	19n	0.4n	1.5n	0.8μ	0.9f	0.5	0.6	-

(b)

Model	R_1 (Ω)	R_2 (Ω)	R_3 (Ω)	R_4 (Ω)	R_5 (Ω)	C_1 (F)	C_2 (F)	C_3 (F)	C_α (F)	C_β (F)	α	β	Z_w ($\Omega s^\alpha(\Omega.S)$)
Ripping	537	808	-	-	-	3n	-	-	-	-	-	-	1447
Cole	7p	1466	-	-	-	-	-	-	0.2μ	-	0.6	-	-
Onion	73	650	6342	915	40380k	0.6n	4.6n	6.5μ	1.5μ	21μ	0.99	0.27	-

(c)

Model	R_1 (Ω)	R_2 (Ω)	R_3 (Ω)	R_4 (Ω)	R_5 (Ω)	C_1 (F)	C_2 (F)	C_3 (F)	C_α (F)	C_β (F)	α	β	Z_w ($\Omega s^\alpha(\Omega.S)$)
Ripping	389	1749	-	-	-	8n	-	-	-	-	-	-	2720
Cole	186	2308	-	-	-	-	-	-	0.26μ	-	0.68	-	-
Onion	38	254	10419	4619	4131	1.2n	1.3n	6.6μ	74p	0.23μ	0.52	0.69	-

(d)

FIGURE 16. *Family$_I$* models parameters corresponding to Fig. 15 for four different *heated* fruits (a) Carrot, (b) Tomato, (c) Zucchini, and (d) Cucumber.

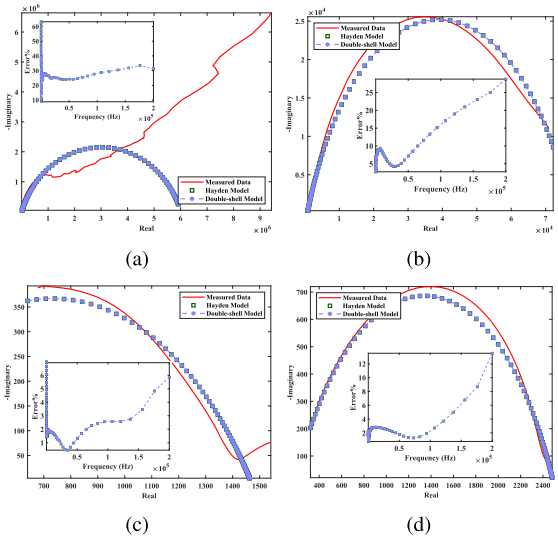

(a) (b) (c) (d)

FIGURE 17. Comparison of some of *Family$_{II}$* models for four different *heated* fruits (a) Carrot, (b) Tomato, (c) Zucchini, and (d) Cucumber.

extraction methods using oscillator circuits were presented in [71]–[73]. The main advantage of using oscillators is that two measurements only are needed to extract all unknown model parameters with the tissue embedded in an oscillator. The authors of [71] used a Wien-brdige oscillator while [73] used sinusoidal and relaxation oscillators successfully combined with the Flower Pollination Algorithm to extract the model parameter values. All in-direct methods are limited to a specific circuit model being chosen prior to the measurements.

Model	R_1 (Ω)	R_2 (Ω)	R_3 (Ω)	C_α (F)	C_β (F)	α	β
Hayden	6011k	11p	-	0.3n	-	0.79	-
Double Shell	17120k	2465k	0	2n	33p	0.73	0.98

(a)

Model	R_1 (Ω)	R_2 (Ω)	R_3 (Ω)	C_α (F)	C_β (F)	α	β
Hayden	77150	734	-	82n	-	0.74	-
Double Shell	72233	1234	0	49n	59n	0.8	0.7

(b)

Model	R_1 (Ω)	R_2 (Ω)	R_3 (Ω)	C_α (F)	C_β (F)	α	β
Hayden	1466	2.5p	-	0.2μ	-	0.6	-
Double Shell	1656	9735	7	4.9μ	0.6μ	0.66	0.63

(c)

Model	R_1 (Ω)	R_2 (Ω)	R_3 (Ω)	C_α (F)	C_β (F)	α	β
Hayden	2494	201	-	0.23μ	-	0.68	-
Double Shell	2467	302	146	0.14μ	9n	0.73	0.85

(d)

FIGURE 18. *Family$_{II}$* models parameters corresponding to Fig. 17 for four different *heated* fruits (a) Carrot, (b) Tomato, (c) Zucchini, and (d) Cucumber.

FIGURE 19. Portable devices for measuring bio-impednace. [58]

C. OPTIMIZATION ALGORITHMS

Once a circuit model is selected, finding its optimal parameter values the minimize the error in magnitude and phase with respect to the measured data becomes an optimization problem. In [74]–[76], new meta-heuristic optimization algorithms were presented to extract bio-impedance model parameters using algorithms like the Flower Pollination Algorithm (FPA) and the Moth-Flame Optimizer (MFO). The performance of these algorithms was compared to the traditional non-linear least square (NLS) and to the Bacterial Foraging Optimization (BFO). Chaotic flower pollination algorithm (CFPA), chaotic grey wolf optimization (CGWO), particle swarm optimization (PSO) and NLS were also compared in [76].

V. CONCLUSION

This survey and literature review summarized most of the widely used bio-impedance models and their applications. A comparison between some of the models was conducted on four different vegetables (Carrot, Tomato, Zucchini, and Cucumber) under three different circumstances (fresh, frozen, and heated). The comparison showed that the Onion model and the Cole model from Family I circuit members had the least error while from Family II members, the Hayden and Double shell models are best suited for this application. It is important to note that measured bio-impedance data must always satisfy the Kramer-Kronig transform pair otherwise, linear circuit models cannot be used to fit this data [77]. Future research in this topic is focused on (i) exploring the possibility of reducing the impedance measurement time by using different types of excitation signals including random signals [78] and (ii) improving optimization algorithms for fitting bio-impedance data such that these algorithms not only report the optimum parameters of a certain model but they automatically search for the best model suitable for a given data [79].

REFERENCES

[1] O. Elwy, A. Abdelaty, L. Said, and A. Radwan, "Fractional calculus definitions, approximations, and engineering applications," *J. Eng. Appl. Sci.*, vol. 67, no. 1, pp. 1–30, 2020.

[2] T. Pritz, "Five-parameter fractional derivative model for polymeric damping materials," *J. Sound Vib.*, vol. 265, no. 5, pp. 935–952, Aug. 2003.

[3] J. Gómez-Aguilar, V. Morales-Delgado, M. Taneco-Hernández, D. Baleanu, R. Escobar-Jiménez, and M. Al Qurashi, "Analytical solutions of the electrical RLC circuit via Liouville–Caputo operators with local and non-local kernels," *Entropy*, vol. 18, no. 8, p. 402, Aug. 2016.

[4] O. Elwy, S. H. Rashad, L. A. Said, and A. G. Radwan, "Comparison between three approximation methods on oscillator circuits," *Microelectron. J.*, vol. 81, pp. 162–178, Nov. 2018.

[5] O. Elwy, L. A. Said, A. H. Madian, and A. G. Radwan, "All possible topologies of the fractional-order wien oscillator family using different approximation techniques," *Circuits, Syst., Signal Process.*, vol. 38, no. 9, pp. 3931–3951, Sep. 2019.

[6] R. Martín, J. J. Quintana, A. Ramos, and I. de la Nuez, "Modeling of electrochemical double layer capacitors by means of fractional impedance," *J. Comput. Nonlinear Dyn.*, vol. 3, no. 2, pp. 61–66, Jan. 2008.

[7] S. Grimnes and O. Martinsen, *Bioimpedance & Bioelectricity Basics*. New York, NY, USA: Academic, 2000.

[8] A. Prasad and M. Roy, "Bioimpedance analysis of vascular tissue and fluid flow in human and plant body: A review," *Biosyst. Eng.*, vol. 197, pp. 170–187, Sep. 2020.

[9] K. S. Cole and R. H. Cole, "Dispersion and absorption in dielectrics I. Alternating current characteristics," *J. Chem. Phys.*, vol. 9, no. 4, pp. 341–351, Apr. 1941.

[10] K. S. Cole, "Permeability and impermeability of cell membranes for ions," in *Proc. Cold Spring Harbor Symp. Quant. Biol.*, vol. 8, 1940, pp. 110–122.

[11] R. I. Hayden, C. A. Moyse, F. W. Calder, D. P. Crawford, and D. S. Fensom, "Electrical impedance studies on potato and alfalfa tissue," *J. Experim. Botany*, vol. 20, no. 2, pp. 177–200, 1969.

[12] A. AboBakr, L. A. Said, A. H. Madian, A. S. Elwakil, and A. G. Radwan, "Experimental comparison of integer/fractional-order electrical models of plant," *AEU-Int. J. Electron. Commun.*, vol. 80, pp. 1–9, Oct. 2017.

[13] M. I. N. Zhang, D. G. Stout, and J. H. M. Willison, "Electrical impedance analysis in plant Tissues3," *J. Experim. Botany*, vol. 41, no. 3, pp. 371–380, 1990.

[14] M. I. N. Zhang and J. H. M. Willison, "Electrical impedance analysis in plant Tissues11," *J. Experim. Botany*, vol. 42, no. 11, pp. 1465–1475, 1991.

[15] M. I. N. Zhang and J. H. M. Willison, "Electrical impedance analysis in plant tissues: *In vivo* detection of freezing injury," *Can. J. Botany*, vol. 70, no. 11, pp. 2254–2258, Nov. 1992.

[16] H. D. Souza and E. E. S. Sampaio, "Apparent resistivity and spectral induced polarization in the submarine environment," *Anais da Academia Brasileira de Ciáncias*, vol. 73, no. 3, pp. 429–444, Sep. 2001.

[17] C. M. Ionescu and R. De Keyser, "Time domain validation of a fractional order model for human respiratory system," in *Proc. 14th IEEE Medit. Electrotechn. Conf.*, May 2008, pp. 89–95.

[18] M. Islam, K. A. Wahid, A. V. Dinh, and P. Bhowmik, "Model of dehydration and assessment of moisture content on onion using EIS," *J. Food Sci. Technol.*, vol. 56, no. 6, pp. 2814–2824, Jun. 2019.

[19] M. Tiitta and H. Olkkonen, "Electrical impedance spectroscopy device for measurement of moisture gradients in wood," *Rev. Sci. Instrum.*, vol. 73, no. 8, pp. 3093–3100, Aug. 2002.

[20] R. L. Magin, *Fractional Calculus Bioengineering*. Redding, MA, USA: Begell House, 2006.

[21] M. H. Jones and J. Scott, "Scaling of electrode-electrolyte interface model parameters in phosphate buffered saline," *IEEE Trans. Biomed. Circuits Syst.*, vol. 9, no. 3, pp. 441–448, Jun. 2015.

[22] J. Scott and P. Single, "Compact nonlinear model of an implantable electrode array for spinal cord stimulation (SCS)," *IEEE Trans. Biomed. Circuits Syst.*, vol. 8, no. 3, pp. 382–390, Jun. 2014.

[23] T. Repo, J. Laukkanen, and R. Silvennoinen, "Measurement of the tree root growth using electrical impedance spectroscopy," *Silva Fennica*, vol. 39, no. 2, 2005, Art. no. 380, doi: 10.14214/sf.380.

[24] P. Ibba, A. Falco, B. D. Abera, G. Cantarella, L. Petti, and P. Lugli, "Bio-impedance and circuit parameters: An analysis for tracking fruit ripening," *Postharvest Biol. Technol.*, vol. 159, Jan. 2020, Art. no. 110978.

[25] T. Repo and M. I. N. Zhang, "Modelling woody plant tissues5," *J. Experim. Botany*, vol. 44, no. 5, pp. 977–982, 1993.

[26] R. Åywica, G. Pierzynowska-Korniak, and J. Wójcik, "Application of food products electrical model parameters for evaluation of apple purée dilution," *J. Food Eng.*, vol. 67, no. 4, pp. 413–418, Apr. 2005.

[27] J. Juansah, I. W. Budiastra, K. Dahlan, and K. B. Seminar, "Electrical behavior of garut citrus fruits during ripening changes in resistance and capacitance models of internal fruits," *Int. J. Eng. Technol.*, vol. 12, no. 4, pp. 1–8, Aug. 2012.

[28] R. R. Nigmatullin and Y. E. Ryabov, "Cole-davidson dielectric relaxation as a self-similar relaxation process," *Phys. Solid State*, vol. 39, no. 1, pp. 87–90, Jan. 1997, doi: 10.1134/1.1129804.

[29] *Bioimpedance Bioelectricity Basics*. Amsterdam, The Netherlands: Elsevier, 2015.

[30] D. J. Bora and R. Dasgupta, "Various skin impedance models based on physiological stratification," *IET Syst. Biol.*, vol. 14, no. 3, pp. 147–159, Jun. 2020.

[31] B. Fu and T. Freeborn, "Electrical equivalent network modeling of forearm tissue bioimpedance," in *Proc. SoutheastConf.*, Apr. 2019, pp. 1–7.

[32] Z. B. Vosika, G. M. Lazovic, G. N. Misevic, and J. B. Simic-Krstic, "Fractional calculus model of electrical impedance applied to human skin," *PLoS ONE*, vol. 8, no. 4, Apr. 2013, Art. no. e59483.

[33] G. Lazovic, Z. Vosika, M. Lazarevic, J. Simic-Krstic, and D. Koruga, "Modeling of bioimpedance for human skin based on fractional distributed-order modified cole model," *FME Trans.*, vol. 42, no. 1, pp. 74–81, 2014.

[34] R. R. Nigmatullin and J. J. Trujillo, "Mesoscopic fractional kinetic equations versus a Riemann–Liouville integral type," in *Advances in Fractional Calculus*. Dordrecht, The Netherlands: Springer, 2007, pp. 155–167.

[35] J. B. Simić-Krstić, A. J. Kalauzi, S. N. Ribar, L. R. Matija, and G. N. Misevic, "Electrical properties of human skin as aging biomarkers," *Experim. Gerontol.*, vol. 57, pp. 163–167, Sep. 2014.

[36] B. Taji, A. D. C. Chan, and S. Shirmohammadi, "Effect of pressure on skin-electrode impedance in wearable biomedical measurement devices," *IEEE Trans. Instrum. Meas.*, vol. 67, no. 8, pp. 1900–1912, Aug. 2018.

[37] K. Dudzinski, M. Dawgul, K. D. Pluta, B. Wawro, W. Torbicz, and D. G. Pijanowska, "Spiral concentric two electrode sensor fabricated by direct writing for skin impedance measurements," *IEEE Sensors J.*, vol. 17, no. 16, pp. 5306–5314, Aug. 2017.

[38] J. Gregory, N. Xi, and Y. Shen, "Towards on-line fingertip bio-impedance identification for enhancement of electro-tactile rendering," in *Proc. IEEE/RSJ Int. Conf. Intell. Robot. Syst.*, Sep. 2009, pp. 3685–3690.

[39] B. Fu and T. J. Freeborn, "Cole-impedance parameters representing biceps tissue bioimpedance in healthy adults and their alterations following eccentric exercise," *J. Adv. Res.*, vol. 25, pp. 285–293, Sep. 2020.

[40] T. J. Freeborn and G. W. Bohannan, "Changes of fractional-order model parameters in biceps tissue from fatiguing exercise," in *Proc. IEEE Int. Symp. Circuits Syst. (ISCAS)*, May 2018, pp. 1–5.
[41] B. Sanchez, J. Li, T. Geisbush, R. B. Bardia, and S. B. Rutkove, "Impedance alterations in healthy and diseased mice during electrically induced muscle contraction," *IEEE Trans. Biomed. Eng.*, vol. 63, no. 8, pp. 1602–1612, Aug. 2016.
[42] B. Sanchez, J. Li, S. Yim, A. Pacheck, J. J. Widrick, and S. B. Rutkove, "Evaluation of electrical impedance as a biomarker of myostatin inhibition in wild type and muscular dystrophy mice," *PLoS ONE*, vol. 10, no. 10, Oct. 2015, Art. no. e0140521.
[43] G. Kumar, U. Kasiviswanathan, S. Mukherjee, S. K. Mahto, N. Sharma, and R. Patnaik, "Changes in electrolyte concentrations alter the impedance during ischemia-reperfusion injury in rat brain," *Physiol. Meas.*, vol. 40, no. 10, Oct. 2019, Art. no. 105004.
[44] M. T. Mbezi, H. Fouda, and C. B. Tabi, "Estimated photosynthetic activity from its electrical impedance spectroscopy," *Amer. Sci. Res. J. Eng., Technol., Sci.*, vol. 13, no. 1, pp. 178–193, 2015.
[45] A. AboBakr, M. Mohsen, L. A. Said, A. H. Madian, A. S. Elwakil, and A. G. Radwan, "Banana ripening and corresponding variations in bio-impedance and glucose levels," in *Proc. Novel Intell. Lead. Emerg. Sci. Conf. (NILES)*, Oct. 2019, pp. 130–133.
[46] G. Knockaert, S. K. Pulissery, L. Lemmens, S. Van Buggenhout, M. Hendrickx, and A. Van Loey, "Carrot β-carotene degradation and isomerization kinetics during thermal processing in the presence of oil," *J. Agricult. Food Chem.*, vol. 60, no. 41, pp. 10312–10319, Oct. 2012.
[47] R. Pearce, "Plant freezing and damage," *Ann. Botany*, vol. 87, no. 4, pp. 417–424, Apr. 2001.
[48] A. Deroeck, D. Sila, T. Duvetter, A. Vanloey, and M. Hendrickx, "Effect of high pressure/high temperature processing on cell wall pectic substances in relation to firmness of carrot tissue," *Food Chem.*, vol. 107, no. 3, pp. 1225–1235, Apr. 2008.
[49] L. Wu, Y. Ogawa, and A. Tagawa, "Electrical impedance spectroscopy analysis of eggplant pulp and effects of drying and freezing–thawing treatments on its impedance characteristics," *J. Food Eng.*, vol. 87, no. 2, pp. 274–280, Jul. 2008.
[50] B. M. Aboalnaga, L. A. Said, A. H. Madian, A. S. Elwakil, and A. G. Radwan, "Cole bio-impedance model variations in daucus carota sativus under heating and freezing conditions," *IEEE Access*, vol. 7, pp. 113254–113263, 2019.
[51] Y. Lee, T. Watanabe, Y. Nakaura, Y. Ando, M. Nagata, and K. Yamamoto, "Cultivar differences in electrical and mechanical property changes and tolerance in apples due to high hydrostatic pressure treatment," *Postharvest Biol. Technol.*, vol. 156, Oct. 2019, Art. no. 110947.
[52] T. Imaizumi, F. Tanaka, D. Hamanaka, Y. Sato, and T. Uchino, "Effects of hot water treatment on electrical properties, cell membrane structure and texture of potato tubers," *J. Food Eng.*, vol. 162, pp. 56–62, Oct. 2015.
[53] Y. Ando, K. Mizutani, and N. Wakatsuki, "Electrical impedance analysis of potato tissues during drying," *J. Food Eng.*, vol. 121, pp. 24–31, Jan. 2014.
[54] T. Watanabe, N. Nakamura, Y. Ando, T. Kaneta, H. Kitazawa, and T. Shiina, "Application and simplification of cell-based equivalent circuit model analysis of electrical impedance for assessment of drop shock bruising in japanese pear tissues," *Food Bioprocess Technol.*, vol. 11, no. 11, pp. 2125–2129, Nov. 2018.
[55] Z. Pengfei, Z. Hanlin, Z. Dongjie, W. Zhijie, F. Lifeng, H. Lan, M. Qin, and W. Zhongyi, "Rapid on-line non-destructive detection of the moisture content of corn ear by bioelectrical impedance spectroscopy," *Int. J. Agricult. Biol. Eng.*, vol. 8, no. 6, pp. 37–45, 2015.
[56] Y. J. Koh, J. Hur, and J. S. Jung, "Postharvest fruit rots of kiwifruit (Actinidia deliciosa) in Korea," *New Zealand J. Crop Horticultural Sci.*, vol. 33, no. 3, pp. 303–310, Sep. 2005.
[57] M. R. Baidillah, D. Kawashima, and M. Takei, "Compensation of volatile-distributed current due to variance of the unknown contact impedance in an electrical impedance tomography sensor," *Meas. Sci. Technol.*, vol. 30, no. 3, Mar. 2019, Art. no. 034002.
[58] A. AboBakr, M. Mohsen, L. A. Said, A. H. Madian, A. S. Elwakil, and A. G. Radwan, "Toward portable bio-impedance devices," in *Proc. 4th Int. Conf. Adv. Comput. Tools Eng. Appl. (ACTEA)*, Jul. 2019, pp. 1–4.
[59] A. A. Al-Ali, A. S. Elwakil, and B. J. Maundy, "Bio-impedance measurements with phase extraction using the kramers-kronig transform: Application to strawberry aging," in *Proc. IEEE 61st Int. Midwest Symp. Circuits Syst. (MWSCAS)*, Aug. 2018, pp. 468–471.
[60] T. J. Freeborn, "Performance evaluation of raspberry pi platform for bioimpedance analysis using least squares optimization," *Pers. Ubiquitous Comput.*, vol. 23, no. 2, pp. 279–285, Apr. 2019.
[61] S. Altaf, S. Ahmad, M. Zaindin, and M. W. Soomro, "Xbee-based WSN architecture for monitoring of banana ripening process using knowledge-level artificial intelligent technique," *Sensors*, vol. 20, no. 14, p. 4033, Jul. 2020.
[62] J.-J. Cabrera-Lopez and J. Velasco-Medina, "Structured approach and impedance spectroscopy microsystem for fractional-order electrical characterization of vegetable tissues," *IEEE Trans. Instrum. Meas.*, vol. 69, no. 2, pp. 469–478, Feb. 2020.
[63] B. Ibrahim, A. Talukder, and R. Jafari, "Multi-source multi-frequency bio-impedance measurement method for localized pulse wave monitoring," in *Proc. 42nd Annu. Int. Conf. IEEE Eng. Med. Biol. Soc. (EMBC)*, Jul. 2020, pp. 3945–3948.
[64] T. J. Freeborn, B. Maundy, and A. Elwakil, "Numerical extraction of cole-cole impedance parameters from step response," *Nonlinear Theory Appl.*, vol. 2, no. 4, pp. 548–561, 2011.
[65] T. J. Freeborn, B. Maundy, and A. Elwakil, "Simplifying cole-impedance extraction from the current-excited step response," in *Proc. IEEE 56th Int. Midwest Symp. Circuits Syst. (MWSCAS)*, Aug. 2013, pp. 952–955.
[66] T. J. Freeborn, B. Maundy, and A. S. Elwakil, "Cole impedance extractions from the step-response of a current excited fruit sample," *Comput. Electron. Agricult.*, vol. 98, pp. 100–108, Oct. 2013.
[67] T. J. Freeborn, B. Maundy, and A. S. Elwakil, "Extracting the parameters of the double-dispersion cole bioimpedance model from magnitude response measurements," *Med. Biol. Eng. Comput.*, vol. 52, no. 9, pp. 749–758, Sep. 2014.
[68] T. J. Freeborn, A. Elwakil, and B. Maundy, "Electrode location impact on cole-impedance parameters using magnitude-only measurements," in *Proc. IEEE 59th Int. Midwest Symp. Circuits Syst. (MWSCAS)*, Oct. 2016, pp. 1–4.
[69] T. J. Freeborn, A. Elwakil, and B. Maundy, "Factors impacting accurate cole-impedance extractions from magnitude-only measurements," in *Proc. IEEE Int. Conf. Syst., Man, Cybern. (SMC)*, Oct. 2016, pp. 223–227.
[70] T. J. Freeborn, A. S. Elwakil, and B. Maundy, "Variability of cole-model bioimpedance parameters using magnitude-only measurements of apples from a two-electrode configuration," *Int. J. Food Properties*, vol. 20, no. sup1, pp. S507–S519, Dec. 2017.
[71] C. Vastarouchas, C. Psychalinos, A. S. Elwakil, and A. A. Al-Ali, "Novel two-measurements-only cole-cole bio-impedance parameters extraction technique," *Measurement*, vol. 131, pp. 394–399, Jan. 2019.
[72] M. Mohsen, L. A. Said, A. H. Madian, A. S. Elwakil, and A. G. Radwan, "Using meta-heuristic optimization to extract bio-impedance parameters from an oscillator circuit," in *Proc. 17th IEEE Int. New Circuits Syst. Conf. (NEWCAS)*, Jun. 2019, pp. 1–4.
[73] M. Mohsen, L. A. Said, A. S. Elwakil, A. H. Madian, and A. G. Radwan, "Extracting optimized bio-impedance model parameters using different topologies of oscillators," *IEEE Sensors J.*, vol. 20, no. 17, pp. 9947–9954, Sep. 2020.
[74] D. A. Yousri, A. M. Abdelaty, L. A. Said, A. AboBakr, and A. G. Radwan, "Biological inspired optimization algorithms for cole-impedance parameters identification," *AEU-Int. J. Electron. Commun.*, vol. 78, pp. 79–89, Aug. 2017.
[75] D. Yousri, A. M. AbdelAty, L. A. Said, and A. G. Radwan, "Biologically inspired optimization algorithms for fractional-order bioimpedance models parameters extraction," in *Fractional Order System*. Amsterdam, The Netherlands: Elsevier, 2018, pp. 125–162.
[76] D. Yousri, A. M. Abdelaty, L. A. Said, A. S. Elwakil, B. Maundy, and A. G. Radwan, "Chaotic flower pollination and grey wolf algorithms for parameter extraction of bio-impedance models," *Appl. Soft Comput.*, vol. 75, pp. 750–774, Feb. 2019.
[77] A. A. Al-Ali, A. S. Elwakil, and B. J. Maundy, "Extraction of bioimpedance phase information from its magnitude using a non-uniform Kramers–Kronig transform," *Eur. Biophys. J.*, vol. 49, no. 2, pp. 207–213, Mar. 2020, doi: 10.1007/s00249-020-01425-0.
[78] S. Majzoub, A. Allagui, and A. S. Elwakil, "Fast spectral impedance measurement method using a structured random excitation," *IEEE Sensors J.*, vol. 20, no. 15, pp. 8637–8642, Aug. 2020.
[79] A. Al-Ali, A. Elwakil, B. Maundy, and D. Westwick, "A generic impedance modeling technique," *AEU - Int. J. Electron. Commun.*, vol. 123, Aug. 2020, Art. no. 153301. [Online]. Available: http://www.sciencedirect.com/science/article/pii/S1434841120302636